

Nonlinear Dynamics and Symbolic Dynamics of Neural Networks

John E. Lewis*

Leon Glass

*Department of Physiology, McGill University,
3655 Drummond Street, Montréal, Québec, Canada H3G 1Y6*

A piecewise linear equation is proposed as a method of analysis of mathematical models of neural networks. A symbolic representation of the dynamics in this equation is given as a directed graph on an N -dimensional hypercube. This provides a formal link with discrete neural networks such as the original Hopfield models. Analytic criteria are given to establish steady states and limit cycle oscillations independent of network dimension. Model networks that display multiple stable limit cycles and chaotic dynamics are discussed. The results show that such equations are a useful and efficient method of investigating the behavior of neural networks.

1 Introduction ---

An understanding of the dynamics of neural networks is essential to the study of many animal behaviors, from such primitive functions as respiration and locomotion to the most sophisticated such as perception and thought. In the past several decades, there have been extensive theoretical analyses complementing purely experimental approaches. In this paper we discuss the properties of theoretical models of neural networks from a perspective of nonlinear dynamics. We analyze qualitative features of the dynamics such as the existence and stability of steady states, cycles, and chaotic dynamics.

Theoretical models of neural networks (Hopfield 1984) in the infinite gain limit can be written as a piecewise linear ordinary differential equation that was studied some years ago (Glass 1975, 1977a,b; Glass and Pasternack 1978). Since a good deal is known about the properties of the piecewise linear equation, this can be immediately translated to the study of neural network models. In Section 2 we motivate and illustrate the results by analyzing a didactic example of a 2 neuron network. In this section we also show how this simple example generalizes to

*Present address: Department of Biology, University of California, San Diego, La Jolla, CA, 92093-0322.

an N -dimensional piecewise linear ordinary differential equation that is equivalent to more familiar theoretical models of neural networks. In Section 3 we discuss the properties of the piecewise linear equation and obtain graphic criteria for stable steady states and limit cycle oscillations. In Section 4 we consider dynamics in several specific networks. We illustrate many different types of dynamics found in these networks with the emphasis on exotic dynamics such as multiple attractors, complex bifurcations, and chaotic dynamics. A preliminary report of some of these results has recently appeared (Lewis and Glass 1991).

2 Theoretical Models of Neural Networks

2.1 A Network with Feedback Inhibition. This section contains a pedagogic example to illustrate the basic ideas of our approach. Consider a network consisting of 2 model neurons whose activities are represented by y_1 and y_2 . We assume that y_1 excites y_2 , but that y_2 inhibits y_1 . This network is modeled by the ordinary differential equation

$$\frac{dy_1}{dt} = -y_1 + 1 - 2H(y_2), \quad \frac{dy_2}{dt} = -y_2 - 1 + 2H(y_1) \quad (2.1)$$

where $H(y)$ is the Heaviside step function

$$H(y) = \begin{cases} 0, & \text{if } y < 0 \\ 1, & \text{if } y \geq 0 \end{cases} \quad (2.2)$$

The equations are piecewise linear and can be integrated analytically. For example, consider a point $[y_1(0), y_2(0)]$ in the positive quadrant. Integrating equation 2.1, we obtain

$$y_1(t) = -1 + [y_1(0) + 1] \exp(-t), \quad y_2(t) = 1 + [y_2(0) - 1] \exp(-t) \quad (2.3)$$

From equation 2.3 we find that the trajectories in the positive quadrant are straight lines given by

$$\frac{y_1(t) + 1}{y_1(0) + 1} = \frac{y_2(t) - 1}{y_2(0) - 1} \quad (2.4)$$

In similar fashion, the trajectories in the other quadrants follow from a direct integration of the equations. In any given quadrant the flow is focused towards a point in the adjacent quadrant in a counterclockwise direction (Fig. 1A). All the focal points lie on one of the vertices of a square centered at the origin.

The limiting behavior as $t \rightarrow \infty$ is determined as follows. Consider an initial point $(s, 0)$ lying on the positive y_1 axis. After passing through all four quadrants the point will be mapped to $[h(s), 0]$ where $h(s)$ is called the Poincaré or return map and is given

$$h(s) = \frac{s}{1 + 4s} \quad (2.5)$$

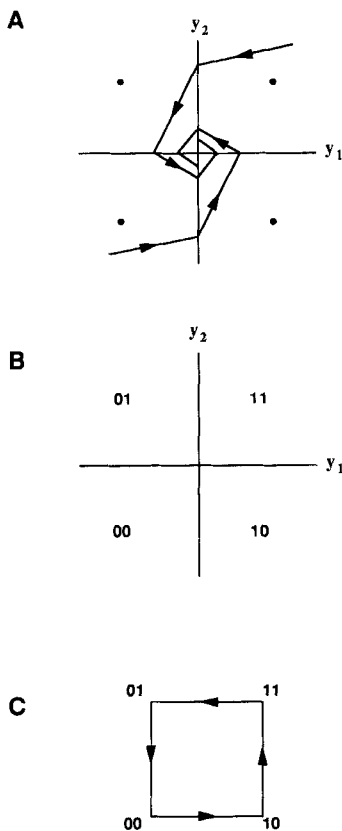


Figure 1: (A) Phase plane portrait of the neural network in equation 2.1. All trajectories are straight lines directed to the focal points indicated by the heavy dots. (B) Coarse grained phase space associating a Boolean state to each of the four quadrants. (C) A directed graph showing the symbolic transitions allowed in this network.

By iterating this map we find that the subsequent images of the initial point approach the origin (Glass and Pasternack 1978). Thus, the flow spirals in toward the origin. This discussion provides a complete analysis of this problem from the perspective of nonlinear dynamics.

Symbolic dynamics provides a complementary method of capturing qualitative features of the flow. In symbolic dynamics one divides the phase space up into coarse regions and gives each a symbol. Instead of the trajectory that gives the values of the variables as a function of time,

the dynamics is given by a sequence of symbols reflecting the coarse grained regions through which the flow passes. In the current case a natural coarse graining is to label each of the four quadrants by a Boolean state as shown in Figure 1B. The flow between the four states is now reflected as a directed graph (Fig. 1C). Thus, in symbolic dynamics the flow is represented as

$$10 \rightarrow 11 \rightarrow 01 \rightarrow 00 \rightarrow 10 \rightarrow \dots$$

The analysis that follows shows several ways in which symbolic dynamics can be used in the analysis of neural networks. We show that (1) restrictions on symbolic transitions can be determined without a detailed numerical or analytical integration of the dynamics but based solely on the logical structure of the network; (2) in some cases the properties of the differential equations can be derived from the symbolic transitions; and (3) symbolic dynamics offers novel ways to classify dynamics.

2.2 N -Dimensional Equations. We now consider vector fields in N dimensions that represent a natural extension of the example in Section 2.1. In N dimensions, Euclidean phase space is subdivided into 2^N regions, called orthants. All the orthants share a common point at the origin. In each orthant the trajectories are straight lines directed from each point of the orthant to a focal point. All the trajectories in each orthant are directed toward the same focal point, but the focal points may be different for the different orthants. The focal points are chosen such that the flows across the boundary between any two adjacent orthants are transverse and are of unique orientation.

Piecewise linear equations, originally proposed by Glass and Pasternack (1978), represent the class of vector fields just described. There are N variables, designated y_i , $i = 1, 2, \dots, n$. For each variable y_i , we define a corresponding Boolean variable, \tilde{y}_i , where

$$\tilde{y}_i = \begin{cases} 0, & \text{if } y_i < 0 \\ 1, & \text{if } y_i \geq 0 \end{cases} \quad (2.6)$$

The equations can be written in terms of the Boolean variables to give

$$\frac{dy_i}{dt} = \Lambda_i(\tilde{y}_1, \dots, \tilde{y}_{i-1}, \tilde{y}_{i+1}, \dots, \tilde{y}_N) - y_i, \quad i = 1, 2, \dots, N \quad (2.7)$$

where for each i the value of $\Lambda_i(\tilde{y}_1, \dots, \tilde{y}_{i-1}, \tilde{y}_{i+1}, \dots, \tilde{y}_N)$ does not depend on \tilde{y}_i , and Λ_i is nowhere 0.

Now we consider neural networks. One popular formulation (Hopfield 1984; Sompolinsky *et al.* 1988; Amit 1989) of neural networks is

$$\frac{dy_i}{dt} = -y_i + \sum_{j=1}^N w_{ij} G_j(y_j) - \tau_i, \quad i = 1, 2, \dots, N \quad (2.8)$$

where N is the number of elements constituting the network, G_i is a nonlinear gain function describing the response of each element to an input, τ_i is a parameter that we interpret as the response threshold, w_{ij} gives the weight of the input of element j to element i , and $w_{ii} = 0$.

It is usual to assume that the nonlinear functions G_j are monotonically increasing or decreasing sigmoidal functions. Consider the limit of infinite slope (or gain) of the sigmoidal function in which the functions G_j are piecewise constant with a single discontinuity at 0, so that

$$G_j(y_j) = \begin{cases} a_j, & \text{if } y_j < 0 \\ b_j, & \text{if } y_j \geq 0 \end{cases} \tag{2.9}$$

with the condition that

$$\sum_{j=1}^N w_{ij}G_j(y_j) \neq \tau_i, \quad i = 1, 2, \dots, N \tag{2.10}$$

Consequently, equations 2.7 and 2.8 are equivalent provided the values of Λ_i are

$$\Lambda_i(\tilde{y}_1, \dots, \tilde{y}_{i-1}, \tilde{y}_{i+1}, \dots, \tilde{y}_N) = \sum_{j=1}^N w_{ij}G_j(y_j) - \tau_i, \quad i = 1, 2, \dots, N \tag{2.11}$$

This analysis shows that commonly used neural network models in the infinite gain limit are a special case of the piecewise linear equations proposed by Glass and Pasternack (1978).

3 Symbolic Dynamics and the State Transition Diagram ---

Some of the qualitative features of the dynamics of equation 2.7 can be appreciated from a symbolic representation of the dynamics on an N -dimensional hypercube, called an N -cube. We now describe some of the properties of N -cubes and then show their connection with the piecewise linear differential equations. Readers may find it useful to refer back to the example discussed in Section 2.1 to see how the concepts apply in a simple case. Several additional examples are given in Section 4.

3.1 The N -Cube. Boolean N -cubes have often been used to represent dynamics in switching networks (Keister *et al.* 1951). A Boolean variable is either 1 or 0. If there are N variables, then a Boolean state is an N -tuple of 1s and 0s designating a value for each variable. For N variables there are 2^N different Boolean states.

For equation 2.7, the N -dimensional Euclidean phase space can be partitioned into 2^N orthants, by the coordinate hyperplanes defined by $y_i = 0$. Each orthant can be labeled by an N -tuple of 1s and 0s, corresponding to the values of \tilde{y}_i from equation 2.6. The N -cube can now be constructed by selecting a single point from each of the 2^N orthants.

Each of these points, called vertices, is labeled by the Boolean N -tuple designating the orthant from which it was derived. Each vertex can be connected to N adjacent vertices associated with Boolean states that differ in 1 locus. The resulting geometric object, called the N -cube, has 2^N vertices and $N \times 2^{N-1}$ edges. The (Hamming) distance between any 2 Boolean states, or vertices on the N -cube, is equal to the number of loci that differ in the 2 states.

3.2 Integration of the Piecewise Linear Equations. From the above discussion every point in phase space is mapped to a vertex of the N -cube. The solution curves of equation 2.7 originating at a point $P = (p_1, p_2, \dots, p_N)$ are given by

$$y_i = \lambda_i + (p_i - \lambda_i) \exp(-t), \quad i = 1, 2, \dots, N \quad (3.1)$$

where

$$\lambda_i = \Lambda_i(\tilde{p}_1, \tilde{p}_2, \dots, \tilde{p}_N) \quad (3.2)$$

Thus, all the local solutions to equation 2.7 in the orthant containing P are straight lines directed to a common focal point $(\lambda_1, \lambda_2, \dots, \lambda_N)$. Each orthant in phase space has an associated focal point, so that the flows are piecewise linear and piecewise focused.

Solving the equation is reduced to connecting the analytical solution curves in equation 3.1 in a piecewise fashion for each element. This entails finding the sequence of times at which the solution trajectory crosses one of the threshold hyperplanes, $y_i = 0$. Given an initial condition $P = (p_1, p_2, \dots, p_N)$ at a time t , the times, t_i ($i = 1, \dots, N$), at which each of the N variables would cross a threshold hyperplane are given

$$t_i(t) = t - \ln \left[\frac{\tau - \lambda_i}{x_i(t) - \lambda_i} \right], \quad i = 1, \dots, N \quad (3.3)$$

Taking the minimum of t_i (over all i) gives the next transition time. To carry out a numerical integration of the system, we compute the next transition time, then update the variables, and iterate the process using equation 3.3 with the new definitions of λ_i .

3.3 The Truth Table and the State Transition Diagram. Based on the above discussion, we have the coarse grained symbolic transition

$$\tilde{p}_1, \tilde{p}_2, \dots, \tilde{p}_N \rightarrow \tilde{\lambda}_1, \tilde{\lambda}_2, \dots, \tilde{\lambda}_N$$

where the first state represents the orthant of the initial point P and the second state represents the orthant of the focal point toward which the flow is directed. The table that gives the symbolic location of the focal point for each orthant is defined here as the truth table.

Now consider the connection between the flows in the piecewise linear equations, and the truth table. Call the current Boolean state S_1 and

the Boolean state toward which the flow is directed, given by the truth table, S_2 . If the distance between S_1 and S_2 is 0, then all initial conditions in orthant S_1 are directed towards the focal point in S_1 leading to a stable steady state in the differential equation. If the distance between S_1 and S_2 is 1 then trajectories from all initial conditions in S_1 are directed across the common boundary between S_1 and S_2 . Now suppose the distance between S_1 and S_2 is greater than 1; for example, let the two states differ in n loci. Then the flow from S_1 can be directed to any of the n different orthants that lie a distance of 1 from S_1 and $n - 1$ from S_2 . The boundary that is crossed depends on the initial condition in S_1 . As a consequence of the above properties the allowed transitions can be represented as a directed graph on an N -cube. This directed graph is called the state transition diagram. As the dynamics of equation 2.7 evolve, the trajectories may pass into different orthants in phase space. Thus a symbolic sequence is generated corresponding to the sequence of orthants visited along the trajectory. These symbolic sequences are consistent with the allowed transitions from the state transition diagram on the N -cube.

The state transition diagram for equation 2.7 has the following property. *Each edge is oriented in one and only one direction.* This can be established using simple arguments (Glass 1975, 1977a,b). Since we assume that for each i the value of $\Lambda_i(\tilde{y}_1, \dots, \tilde{y}_{i-1}, \tilde{y}_{i+1}, \dots, \tilde{y}_N)$ does not depend on \tilde{y}_i (i.e., $w_{ii} = 0$), an edge cannot be directed in two directions. From the construction of the state transition diagram, the number of directed edges in the state transition diagram is equal to the distance between each state on the left-hand side of the truth table, and the subsequent state on the right-hand side. Each column on the right-hand side of the truth table contributes 2^{N-1} to the total distance, and there are N columns so that the total distance is $N \times 2^{N-1}$. This is equal to the total number of edges of the N -cube. Since no edge can be oriented in 2 directions, it follows that every edge has one unique orientation.

3.4 Steady States and Limit Cycles. A problem of general interest is to make assertions concerning the qualitative dynamics of equation 2.7 based solely on the state transition diagram. Previous work established rules to find stable steady states and limit cycles (Glass and Pasternack 1978). Very briefly, if the N edges at any given vertex of the N -cube are all directed toward it, then in the corresponding orthant of phase space there will be a stable steady state. These steady states, which are called extremal steady states, have been the main focus in the study of neural networks (Cowan and Sharp 1988). For an oscillation to result, a necessary condition is that there be a cyclic path in the state transition diagram. This is not, however, a sufficient condition to guarantee stability or uniqueness of the oscillation. In some circumstances, a much more powerful result can be found. A *cyclic attractor* is defined as a configuration on the N -cube that is analogous to a stable limit cycle in a differential equation. A *cyclic attractor* of length n is a cyclic path through n vertices

of the N -cube such that (1) the edge between successive vertices on the cycle is directed from one to the next in sequence; (2) for any vertex on the cycle, there are $N - 2$ adjacent vertices that are not on the cycle, and the edge(s) from each of these adjacent vertices is(are) directed toward the cycle. If there is a cyclic attractor in the state transition diagram then in the associated piecewise linear differential equations there is either a stable unique limit cycle in phase space such that all points in all orthants associated with the cyclic attractor approach the limit cycle in the limit $t \rightarrow \infty$, or there is an asymptotic oscillatory approach to a point P_f . The point P_f is analogous to a stable focus with each of the n coordinates involved in the cyclic attractor approaching zero. The proof of this result relies on the explicit algebraic computation of the limiting properties of the Poincaré map, giving the return to a threshold hyperplane. The Poincaré map is

$$f(z) = \frac{Az}{1 + \langle \phi, z \rangle} \quad (3.4)$$

where z is an $(N - 1)$ vector on a threshold hyperplane, A is an $(N - 1) \times (N - 1)$ positive matrix, ϕ is a nonnegative $(N - 1)$ vector, and the brackets represent the inner product. For this system, the limiting properties of equation 3.4 on iteration follow using the Perron theorem (Glass and Pasternack 1978).

3.5 Chaotic Dynamics. Chaotic dynamics are aperiodic dynamics in a deterministic system in which there is a sensitivity to the initial state of the system so that two initial conditions, arbitrarily close to one another diverge exponentially over time (Ruelle 1989). Since the flow in any given orthant is always focused toward a single point, it is not obvious that equation 2.7 can display chaotic dynamics. However, as we will show in Section 4 [see also Lewis and Glass (1991)], numerical integration shows chaotic dynamics in some systems. We have not yet found criteria for chaotic dynamics based on the state transition diagram on the N -cube.

4 Dynamics in Model Networks

In this section we illustrate the dynamics that we have observed so far in equation 2.7. Since we are interested in neural networks, we assume the special case given by equations 2.8 and 2.9, and we assume unless otherwise stated that for all j , the functions $G_j(y_j)$ are the same with $a_j = 1$ and $b_j = 0$, and $\tau_i = \tau$ for all i . Likewise all terms of the connection matrix, w_{ij} , are either 1 or 0. Each of the N elements in the network has the same number of inputs, n_p .

Example 1: Steady States. Consider the network in Figure 2A, where the symbol $y_2 \dashv y_1$ implies y_2 inhibits y_1 ($w_{12} = -1$) and $\tau = 0.5$. The integration of the dynamics starting from several initial conditions is

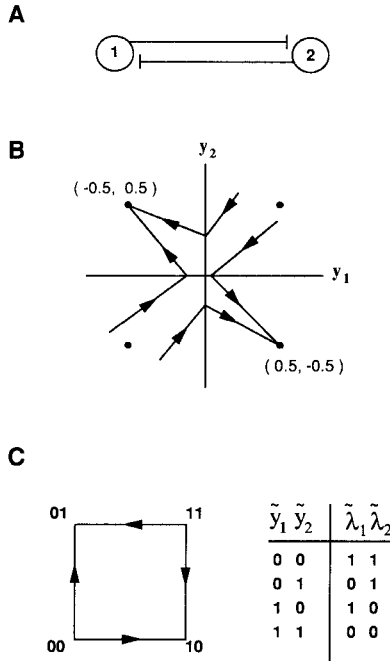


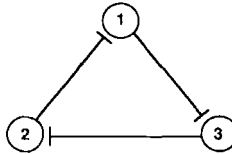
Figure 2: (A) Schematic diagram of a neural network in which there is mutual inhibition. (B) Integration of the PL equations in the phase plane, $\tau = 0.5$. The heavy dots indicate the focal points. (C) State transition diagram on the 2-cube $(\tilde{y}_1, \tilde{y}_2)$ and the associated truth table.

shown in Figure 2B, and the N -cube state transition diagram and truth table are shown in Figure 2C. There are two stable steady states.

Example 2: Stable Limit Cycle. A second example is the cyclic inhibitory loop shown in Figure 3A with $N = 3$. For $\tau = 0.5$, this system gives a unique stable limit cycle oscillation, associated with the cyclic attractor in the state transition diagram (Fig. 3B) (Glass 1975, 1977a,b; Glass and Pasternack 1978). Classification of stable limit cycles using the result in Section 3.4 has been considered previously. The number of distinct cyclic attractors under the symmetry of the N -cube is 1, 1, 3, 18 in dimensions 2, 3, 4, 5, respectively (Glass 1977a).

Example 3: Multiple Limit Cycles in a 5-D Network. Now consider the dynamics of the 5-element network shown in Figure 4A ($n_p = 2$) with $\tau \in (1, 2)$. The state transition diagram for this network is shown in

A



B

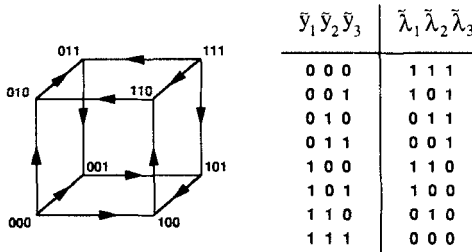


Figure 3: (A) Schematic diagram of a neural network composed of 3 elements. (B) State transition diagram on the 3-cube ($\tilde{y}_1 \tilde{y}_2 \tilde{y}_3$) and the associated truth table. There is a cyclic attractor passing through the states 001, 101, 100, 110, 010, 011.

Figure 4B. Let each vertex on one 4-cube represent all the vertices of the 5-cube in which the first digit of the 5-tuple is 0 and each vertex on the other 4-cube represent all the vertices of the 5-cube in which the first digit is 1. Each vertex on one 4-cube is connected to the equivalent vertex on the other.

From numerical integration, there are 8 stable cycles that have different symbolic sequences for the range of τ considered. The sequences of states for each of these cycles are shown in Table 1, and can also be followed on the state transition diagram. Each state is represented by the 5-tuple $\tilde{y}_1 \tilde{y}_2 \tilde{y}_3 \tilde{y}_4 \tilde{y}_5$.

Figure 4: Facing page. (A) The 5-element network described in Example 3. All connections are inhibitory and of uniform magnitude (i.e., $w_{ij} = 1$). (B) The state transition diagram for the network in (A). The upper 4-cube represents all states in which the first locus is 1; the lower 4-cube represents all states in which the first locus is 0. See text for a more detailed description.

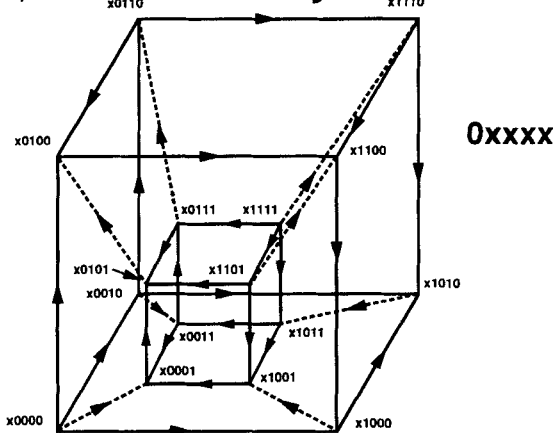
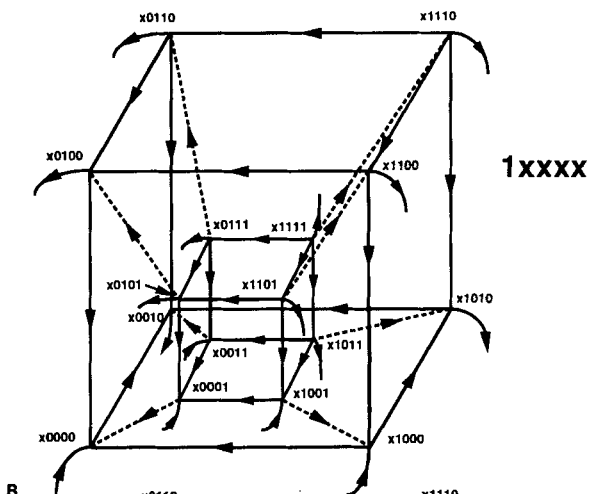
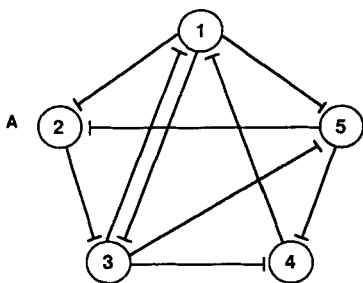


Table 1: Limit Cycles in Example 3.

Cycle 1	Cycle 2	Cycle 3	Cycle 4	Cycle 5	Cycle 6	Cycle 7	Cycle 8
10010	10010	10010	10010	10010	10010	10010	11010
00010	00010	00010	00010	00010	00010	00010	01010
00011	01010	00011	00011	01010	00011	00011	01011
00111	01011	00111	00001	01011	00111	00111	00011
00101	00011	00110	00101	00011	00110	00110	00111
00100	00111	01110	00100	00001	00100	01110	00101
01100	00101	01100	01100	00101	01100	01010	00100
01000	00100	01000	01000	00100	01000	01011	01100
01001	01100	01010	01001	01100	01010	01001	01000
11001	01000	01011	00001	01000	01011	11001	01001
10001	01001	01001	10001	01001	01001	10001	11001
10000	11001	11001	10000	11001	00001	10000	11000
	11000	10001		11000	10001		
	11010	10000		10000	10000		

The stability of each of these cycles depends on the value of τ . For example, Figure 5 shows the three different stable cycles for $\tau = 1.9$. From left to right the panels show the time series corresponding to cycle 4, 5, and 6 from Table 1. To illustrate the bifurcations, we consider the returns to a 4-dimensional face \mathcal{F}_3 separating two neighboring orthants in phase space. The state transition diagram can be used to choose \mathcal{F}_3 . In this example, there is not one state transition that is common to all 8 cycles. However, the transition $01100 \rightarrow 01000$ is common to all cycles except cycle 7. By plotting the point of intersection of the trajectory with this hyperplane as the value of τ is varied for different initial conditions, the regions of parameter space for which each of the 8 cycles are stable can be observed. Projections of the bifurcation diagram constructed in this way onto the y_i -axes are shown in Figure 6. In such diagrams, more than one branch for a given value of τ indicates that either there are multiple cycles, or that one or more cycles have multiple crossings of \mathcal{F}_3 . In Figure 6, each different branch represents a unique cycle. We have numerically analyzed the bifurcations shown here. Briefly, the bifurcation occurring near $\tau = 1.29$ appears to be a subcritical Hopf bifurcation. Increasing τ above this value causes cycles 2 and 3 to lose stability (upper and lower branches). Cycle 1 maintains its stability through this point (middle branch). Near $\tau = 1.66$, an exchange of stability from cycle 1 to cycle 4 occurs. Cycles 5 and 6 gain stability near $\tau = 1.79$ in a bifurcation that is similar to that occurring with cycles 2 and 3 for $\tau = 1.29$. Cycles 7 and 8 are stable for values of $\tau \in (1, 1.25)$.

Cycles 5 and 6 are identical under a relabeling transformation. To make this more clear, consider the sequences of the state transitions in

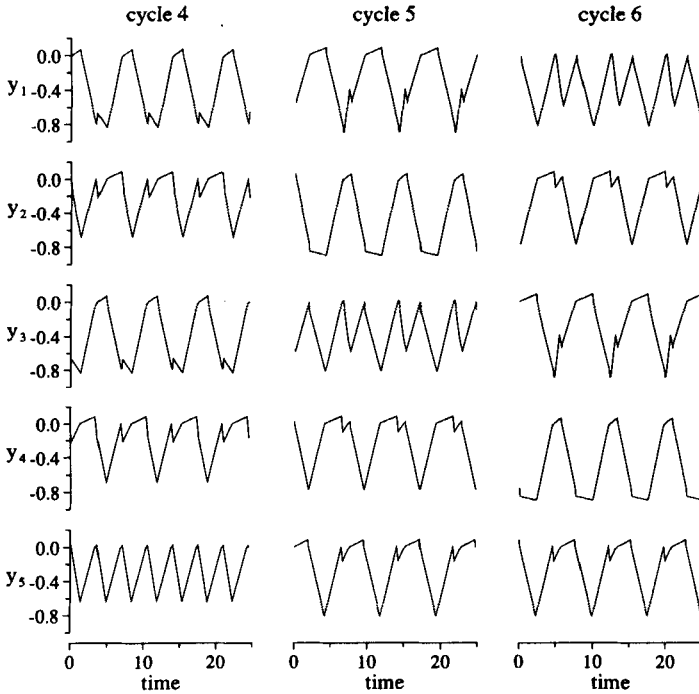


Figure 5: Multistability of cycles for the network described in Example 3 (Fig. 4A). Three different cycles are stable for $\tau = 1.9$ and are shown here by choosing three different initial conditions. The time axis is arbitrary.

Table 1 corresponding to the two cycles. As mentioned earlier, each state is represented by the 5-tuple $\tilde{y}_1\tilde{y}_2\tilde{y}_3\tilde{y}_4\tilde{y}_5$. The relabeling transformation is the following: switch locus 1 with 3 and locus 2 with 4. In other words, the 5-tuple $\tilde{y}_1\tilde{y}_2\tilde{y}_3\tilde{y}_4\tilde{y}_5$ becomes $\tilde{y}_3\tilde{y}_4\tilde{y}_1\tilde{y}_2\tilde{y}_5$. Performing this transformation on one of the cycles shows that the sequences of state transitions are the same, and thus the cycles are the same. This symmetry is also evident in the connectivity of the network (Fig. 4A). A similar relationship exists between cycles 2 and 3 and cycles 7 and 8.

Example 4: Chaotic Dynamics in a 6-D Network. The 6-element network ($n_p = 3$) in Figure 7 exhibits chaotic dynamics for some parameters. A projection of the attractor onto the y_2 - y_4 plane is shown in Figure 8A. We consider a face, \mathcal{F}_4 separating the orthants defined by 011011 and 010011. Figure 8B shows the density histogram for the times between

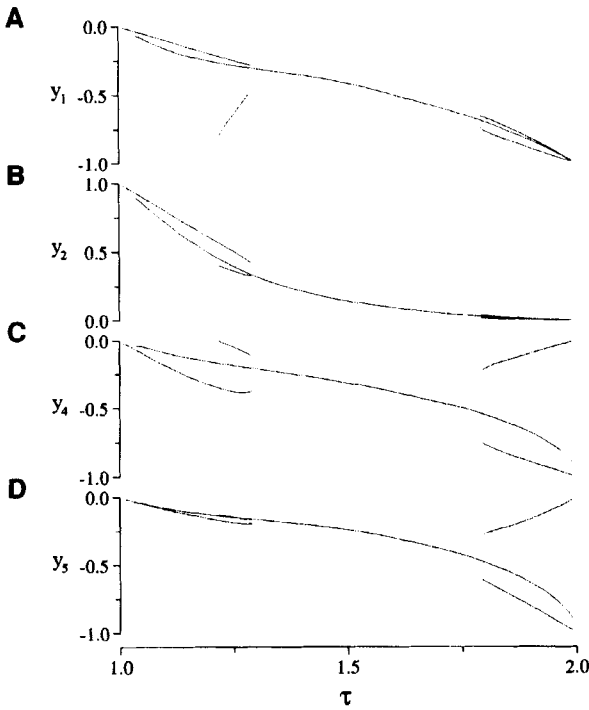


Figure 6: Bifurcation diagram for returns to the face \mathcal{F}_3 and values of τ from 1.001 to 1.999 in steps of 0.001. Each panel (A–D) shows the projections onto the different axes.

2000 successive returns to \mathcal{F}_4 and Figure 8C shows the density for a single variable y_4 on each return to \mathcal{F}_4 . We also consider the evolution of the density histograms for successive returns to \mathcal{F}_4 for a set of 2000 initial conditions in which y_4 was varied, and the other variables were held constant. Figure 8D–F shows that by the 20th return, the histograms have reached a density that is the same as that of a single trajectory (Fig. 8C). The approach to an invariant density and the observation of the same invariant density along a single trajectory constitute numerical evidence that this system is ergodic and has a unique invariant density, two features common to many chaotic systems (Lasota and Mackey 1985).

Now we consider the effects of varying τ on the dynamics of this network. The dynamics are tracked by plotting the values of y_4 on 30 successive crossings of \mathcal{F}_4 as τ is varied. Figure 9A shows the resulting bifurcation diagram. As τ is increased from $\tau = 1.2$, the dynamics change

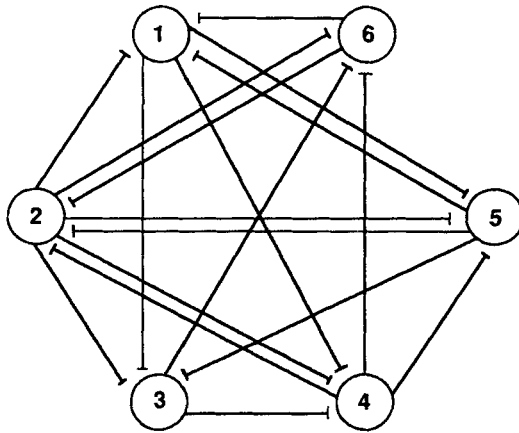


Figure 7: The 6-element network discussed in Example 4.

from a simple limit cycle to aperiodic behavior. For larger values of τ , a limit cycle is evident again. In the aperiodic region, there are at least 4 periodic windows, spaced nearly symmetrically about $\tau = 1.5$. This simple example shows how τ can influence the network dynamics.

Since the step function nonlinearity in equation 2.9 is not realistic as a model for most biological processes, it is important to clarify the dynamics when continuous nonlinear functions are used in equation 2.8. We consider the continuous gain function,

$$G_j(y_j) = \frac{1 + \tanh(-\beta y_j)}{2} \quad (4.1)$$

where β is a positive constant, and equation 4.1 approaches a step function in the limit $\beta \rightarrow \infty$. A 4th order Runge–Kutta integration scheme ($\Delta t = 0.01$) was used to solve the equations.

As the value of β increases, the continuous system exhibits a complex sequence of bifurcations. By using a method similar to that described for Example 3, a bifurcation diagram was constructed for values of β between 7.0 and 12.0 (Fig. 9B). The value of y_4 is plotted as the solution trajectory crosses the $y_3 = 0$ hyperplane in a negative sense. For each value of β , a transient of 300 crossings was allowed before the next 30 points were plotted. A different example of a chaotic 6-dimensional network also shows a complex sequence of bifurcations as a continuous sigmoidal function is steepened (Lewis 1991; Lewis and Glass 1991). Further study of the bifurcations in these systems is needed.

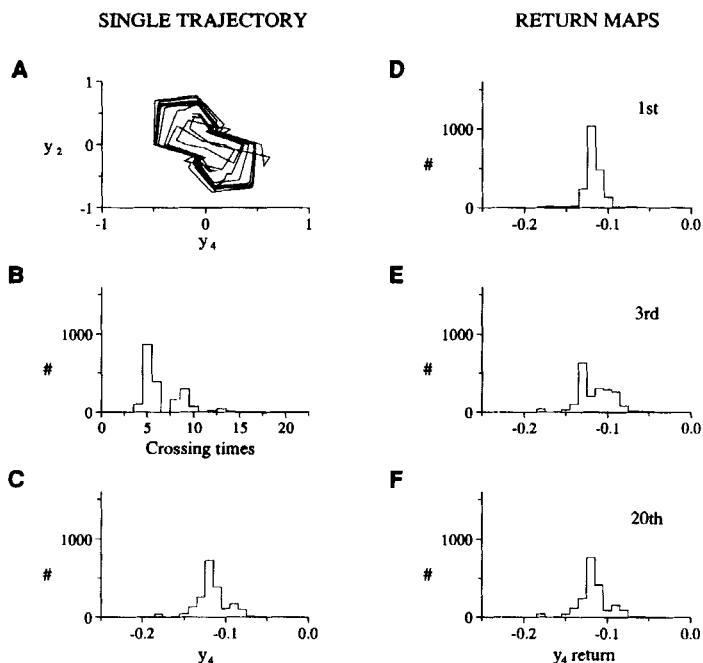


Figure 8: (A) Projection of the dynamics onto the y_2 - y_4 plane for $\tau = 1.5$. (B) shows the density histogram for the times between successive crossings of \mathcal{F}_4 . (C) The density histogram of y_4 for 2000 successive crossings of \mathcal{F}_4 on a single trajectory. (D-F) The density histograms of y_4 for the 1st, 3rd, and 20th returns to \mathcal{F}_4 using 2000 different initial conditions in which equally spaced values of y_4 were chosen between -0.2 and 0 , with $y_1 = -0.293862$, $y_2 = 0.478693$, $y_3 = 0.0$, $y_5 = 0.028766$, and $y_6 = 0.270764$.

Example 5: Chaotic Dynamics in a Network of 50 Elements. We now consider the dynamics of a larger network consisting of 50 elements with $n_p = 5$ and $\tau = 2.5$. Details concerning the network are in Lewis (1991) and will be provided on request. In this network, a search of 100 randomly chosen initial conditions revealed no steady states or limit cycles. As in previous examples, the value of a single variable on the return of the trajectory to an $(N - 1)$ -dimensional face, \mathcal{F}_5 , is considered. Figure 10A shows the density histograms of y_1 on \mathcal{F}_5 (left panel) and the times between returns (right panel) for 500 successive returns of a single trajectory. Figure 10B shows the density histograms for y_1 and the return times for a first return map constructed by taking initial condi-

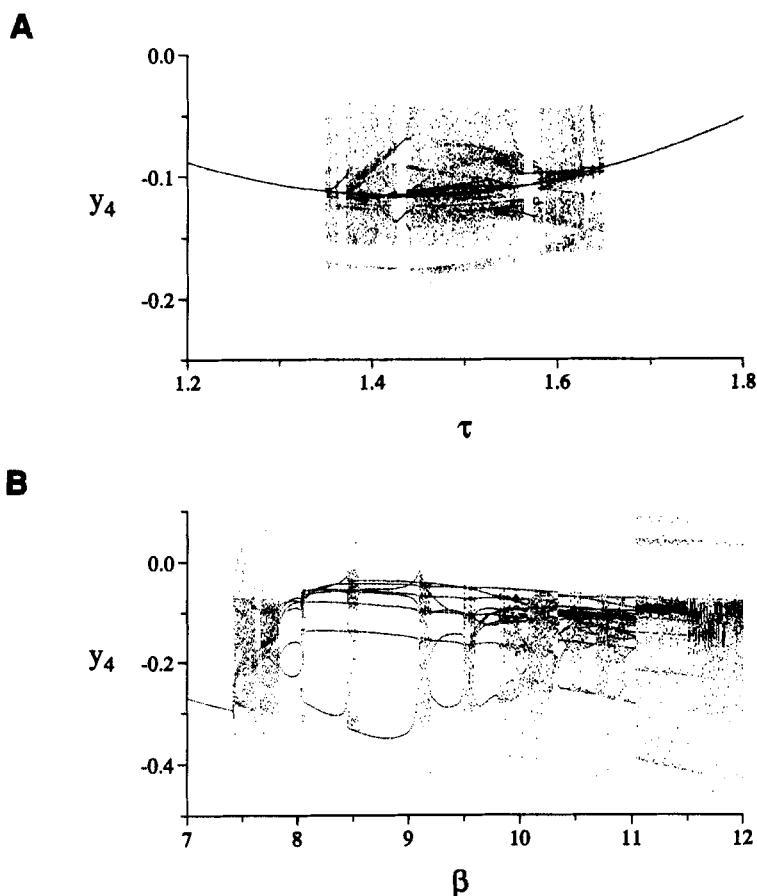


Figure 9: (A) Bifurcation diagram showing the value of y_4 on 30 successive crossings of \mathcal{F}_4 after a sufficient transient, for different values of τ . (B) Bifurcation diagram as a function of β for the continuous network described in Example 4. After a transient, the values of y_4 are plotted when the trajectory crosses the $y_3 = 0$ hyperplane in a negative sense, 30 consecutive times.

tions on \mathcal{F}_5 where all initial values were constant except y_1 which was varied from -3.0 to -1.0 (as in Example 4). These density histograms are similar to those of a single trajectory (Fig. 10A) after only one return to \mathcal{F}_5 . Calculating a first return map for a smaller interval of y_1 , between -2.1 and -1.9 , again reveals similar density histograms (Fig. 10C). This

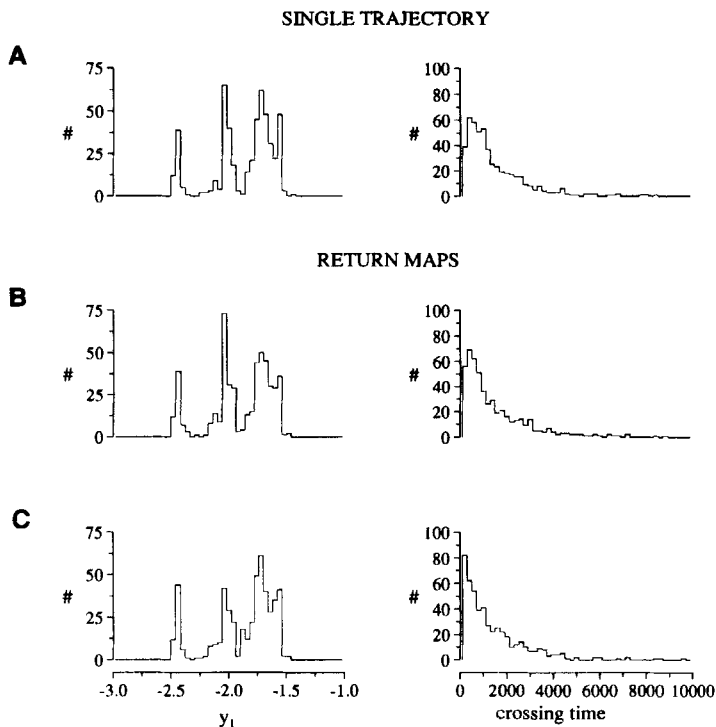


Figure 10: (A) Left panel: The density histogram of y_1 on \mathcal{F}_5 for 500 successive crossings of a single trajectory. Right panel: The density histogram for the corresponding times between successive crossings of \mathcal{F}_5 . (B) Left panel: The density histogram of y_1 on the first return map constructed for 500 different initial conditions on \mathcal{F}_5 in which the value of y_1 was varied between -3.0 and -1.0 . Right panel: The density histogram of the corresponding crossing times for the data in the left panel. (C) Same as (B) but using initial values of y_1 between -2.1 and -1.9 .

system is chaotic and only a small number of passes through phase space is required for nearby trajectories to diverge.

5 Discussion

Neural networks in nature display a wide range of complex dynamic behavior, ranging from more or less regular periodic behavior, to complex fluctuation that is difficult to characterize. The current paper shows that

complex dynamics can also be found in commonly used mathematical models for neural networks. The dynamics can be classified by using the state transition diagram, which links the wiring diagram of the neural network to the coarse-grained activity patterns in the network. The simple structure of the mathematical equations enables us to demonstrate uniqueness and stability of limit cycle oscillations in some special circumstances. We comment briefly on the various dynamics found in these networks. We then discuss some open theoretical questions.

The extremal steady states in these networks are easily identified using the state transition diagram. Recent theoretical studies (Amit 1989) have linked such steady states with memories in neural networks, but we are not aware of physiological studies supporting such an identification.

Neural network limit cycle oscillations have been proposed as models for rhythmogenesis in a large variety of invertebrate and vertebrate systems (Friesen and Stent 1978; Matsuoka 1985). These studies considered networks of a specific connectivity and some analytical results have been obtained for the oscillatory properties of these systems (Matsuoka 1985; Cohen 1988). The current approach provides techniques for associating patterns of oscillation with the underlying connectivity of the network (Glass and Young 1979).

A novel behavior demonstrated here is multistability of limit cycle oscillations, where parameter changes of the network can lead to changes in the stability of the various behaviors (Figs. 5 and 6). This behavior is interesting in light of recent experimental studies on multifunctional invertebrate neural networks (Harris-Warrick and Marder 1991; Meyrand *et al.* 1991), where different types of oscillatory behaviors can be exhibited by a single network.

The simple networks here also support chaotic dynamics. Although the possible role of chaotic dynamics in normal and pathological functioning in neurobiology was raised several years ago (Guevara *et al.* 1983; Harth 1983) clear identification of chaos in neural systems has been possible only in rather simple systems in which there is a periodic forcing of neural tissue (Matsumoto *et al.* 1987; Takahashi *et al.* 1990). There have also been claims that neural activity in more complex situations is chaotic (Rapp *et al.* 1985; Skarda and Freeman 1987; Babloyantz and Destexhe 1987).

The existence of chaotic dynamics in models of abstract neural networks has also been investigated. Kürten and Clark (1986) used spectral and dimensional analysis to identify chaos in a neural network model of 26 elements, each described by 2 ordinary differential equations and interconnected in a pseudorandom manner with each element receiving 7 inputs (both excitatory and inhibitory). Sompolinsky *et al.* (1988) have shown that some continuous models of neural networks will show a transition to chaotic dynamics as a gain parameter is varied. They proved this result in the thermodynamic limit (i.e., in an infinitely large network). Finally, Kepler *et al.* (1990) showed that for a specific formulation

of a neural network implemented as an electronic circuit, chaotic dynamics could be observed in three dimensions. Their investigation focused, however, on the dynamics of four-dimensional networks. A compelling question is to identify and classify network connectivities that are capable of generating chaotic dynamics.

Several mathematical questions are raised by this work. Previously we reported that assuming the same connection parameters for each element (i.e., $w_{ij} = 1$ and n_p inputs to each element), the lowest dimension in which chaotic dynamics was observed is 6 (Lewis and Glass 1991). However, when the w_{ij} are randomly chosen real numbers (with $w_{ij} = 0$), some networks of 5 elements have shown such behavior (less than 0.05% of networks tested). The general system, equation 2.7 has shown chaos in dimensions 4 and higher; in these cases the truth tables consisted of functions that do not correspond to those possible in neural network models. Preliminary studies of the prevalence of the various sorts of dynamic behavior have been carried out. For 2 and 3 input systems in dimension up to 20, chaotic dynamics appear to be a relatively rare phenomenon found in less than 1% of trials in which there were 20 initial conditions for each of 1000 different networks. The number of different attractor basins in these networks is also very small (usually less than 10 attractors, even in dimension 20). However, systematic numerical studies require searching in huge parameter spaces, since one is interested in studying the effects of the numbers of inputs, the thresholds, and the connectivity. The simplicity of numerically integrating the piecewise linear equations facilitate such studies.

A difficult mathematical question is to analyze the bifurcations as the piecewise linear functions are replaced by continuous functions. Numerical results indicate that in systems with cyclic attractors, the limit cycles maintain stability over a large range of steepness of the sigmoidal function, but there is no proof of this (Glass 1977b). The bifurcations in more complex networks that display chaos require further analysis. An especially interesting question is how chaos arises in these systems whose dynamics are dissipative within every coarse-grained orthant of phase space.

This work provides a conceptually simple way to correlate the connectivity and dynamics of simple models of neural networks. This provides a foundation for the investigation of more realistic models of neural networks and complex rhythms observed in the laboratory.

Acknowledgments

This research has been supported by funds from the Natural Sciences and Engineering Research Council of Canada and the Fonds F. C. A. R. du Québec.

References

- Amit, D. J. 1989. *Modeling Brain Function: The World of Attractor Neural Networks*. Cambridge University Press, Cambridge.
- Babloyantz, A., and Destexhe, A. 1987. Chaos in neural networks. *Proc. Int. Conf. Neural Networks*, San Diego, CA, pp. 1–9.
- Cohen, M. A. 1988. Sustained oscillations in a symmetric cooperative-competitive neural network: Disproof of a conjecture about content addressable memory. *Neural Networks* **1**, 217–221.
- Cowan, J. D., and Sharp, D. H. 1988. Neural nets. *Q. Rev. Biophys.* **21**, 305–427.
- Friesen, W. O., and Stent, G. S. 1978. Neural circuits for generating rhythmic movements. *Annu. Rev. Biophys. Bioeng.* **7**, 37–61.
- Glass, L. 1975. Combinatorial and topological methods in nonlinear chemical kinetics. *J. Chem. Phys.* **63**, 1325–1335.
- Glass, L. 1977a. Combinatorial aspects of dynamics in biological systems. In *Statistical Mechanics and Statistical Methods in Theory and Application*, U. Landman, ed., pp. 585–611. Plenum, New York.
- Glass, L. 1977b. Global analysis of nonlinear chemical kinetics. In *Statistical Mechanics, Pt. B*, B. J. Berne, ed., pp. 311–349. Plenum, New York.
- Glass, L., and Pasternack, J. S. 1978. Stable oscillations in mathematical models of biological control systems. *J. Math. Biology* **6**, 207–223.
- Glass, L., and Young, R. 1979. Structure and dynamics of neural network oscillators. *Brain Res.* **179**, 207–218.
- Guevera, M. R., Glass, L., Mackey, M. C., and Shrier, A. 1983. Chaos in neurobiology. *IEEE Trans. Syst. Man Cybern.* **SMC-13**, 790–798.
- Harris-Warrick, R. M., and Marder, E. 1991. Modulation of neural networks for behavior. *Annu. Rev. Neurosci.* **14**, 39–57.
- Harth, E. 1983. Order and chaos in neural systems: Approach to the dynamics of higher brain functions. *IEEE Trans. Syst. Man Cybern.* **SMC-13**, 782–789.
- Hopfield, J. J. 1984. Neurons with graded response have collective computational properties like those of two-state neurons. *Proc. Natl. Acad. Sci. U.S.A.* **81**, 3088–3092.
- Keister, W., Ritchie, A. E., and Washburn, S. H. 1951. *The Design of Switching Circuits*. D. Van Nostrand, Toronto.
- Kepler, T. B., Datt, S., Meyer, R. B., and Abbott, L. F. 1990. Chaos in a neural network circuit. *Physica D* **46**, 449–457.
- Kürten, K. E., and Clark, J. W. 1986. Chaos in neural systems. *Phys. Lett. A* **114**, 413–418.
- Lasota, A., and Mackey, M. C. 1985. *Probabilistic Properties of Deterministic Systems*. Cambridge University Press, Cambridge.
- Lewis, J. E. 1991. Dynamics of neural networks and respiratory rhythm generation. M.Sc. Thesis, McGill University.
- Lewis, J. E., and Glass, L. 1991. Steady states, limit cycles, and chaos in models of complex biological networks. *Int. J. Bifurc. Chaos.* **1**, 477–483.
- Matsumoto, G., Aihara, K., Hanyu, Y., Takahashi, N., Yoshizawa, S., and Nagumo, J. 1987. Chaos and phase locking in normal squid axons. *Phys. Lett. A* **123**, 162–166.

- Matsuoka, K. 1985. Sustained oscillations generated by mutually inhibiting neurons with adaptation. *Biol. Cybern.* **52**, 367–376.
- Meyrand, P., Simmers, J., and Moulins, M. 1991. Construction of a pattern generating circuit with neurons of different networks. *Nature (London)* **351**, 60–63.
- Rapp, P., Zimmerman, I. D., Albano, A. M., deGuzman, G. C., Greenbaum, N. N., and Bashore, T. R. 1985. Experimental studies of chaotic neural behavior: Cellular activity and electroencephalographic signals. In *Nonlinear Oscillations in Biology and Chemistry*, H. G. Othmer, ed., pp. 175–205. Springer-Verlag, Berlin.
- Ruelle, D. 1989. *Chaotic Evolution and Strange Attractors*. Cambridge University Press, Cambridge.
- Skarda, C. A., and Freeman, W. J. 1987. How brains make chaos in order to make sense of the world. *Behav. Brain Sci.* **10**, 161–195.
- Sompolinsky, H., Crisanti, A., and Sommers, H. J. 1988. Chaos in random neural networks. *Phys. Rev. Lett.* **61**, 259–262.
- Takahashi, N., Hanyu, Y., Musha, T., Kubo, R., and Matsumoto, G. 1990. Global bifurcation structure in periodically stimulated giant axons of squid. *Physica D* **43**, 318–334.

Received 19 August 1991; accepted 3 January 1992.